analytical chemistry

Article

pubs.acs.org/ac

Measuring Melittin Uptake into Hydrogel Nanoparticles with Near-Infrared Single Nanoparticle Surface Plasmon Resonance Microscopy

Kyunghee Cho, Jennifer B. Fasoli, Keiichi Yoshimatsu, Kenneth J. Shea, and Robert M. Corn*

Department of Chemistry, University of California−Irvine, Irvine, California 92697, United States

Supporting Information

ABSTRACT: This paper describes how changes in the refractive index of single hydrogel nanoparticles (HNPs) detected with near-infrared surface plasmon resonance microscopy (SPRM) can be used to monitor the uptake of therapeutic compounds for potential drug delivery applications. As a first example, SPRM is used to measure the specific uptake of the bioactive peptide melittin into *N*-isopropylacrylamide (NIPAm)-based HNPs. Point diffraction patterns in sequential real-time SPRM differential reflectivity images are counted to create digital adsorption binding curves of single 220 nm HNPs from picomolar nanoparticle solutions onto hydrophobic alkanethiol-modified gold surfaces. For each digital adsorption binding curve, the average single nanoparticle SPRM reflectivity response, $\langle \Delta\%R_{NP} \rangle$, was measured. The value of $\langle \Delta\%R_{NP} \rangle$ increased linearly from 1.04 ± 0.04 to 2.10 ± 0.10% when the melittin concentration in the HNP solution varied from zero to 2.5 μM. No change in the average HNP size in the presence of melittin is observed with dynamic light scattering measurements, and no increase in $\langle \Delta\%R_{NP} \rangle$ is observed in the presence of either FLAG octapeptide or bovine serum albumin. Additional bulk fluorescence measurements of melittin uptake into HNPs are used to estimate that a 1% increase in $\langle \Delta\%R_{NP} \rangle$ observed in SPRM corresponds to the incorporation of approximately 65000 molecules into each 220 nm HNP, corresponding to roughly 4% of its volume. The lowest detected amount of melittin loading into the 220 nm HNPs was an increase in $\langle \Delta\%R_{NP} \rangle$ of 0.15%, corresponding to the absorption of 10000 molecules.

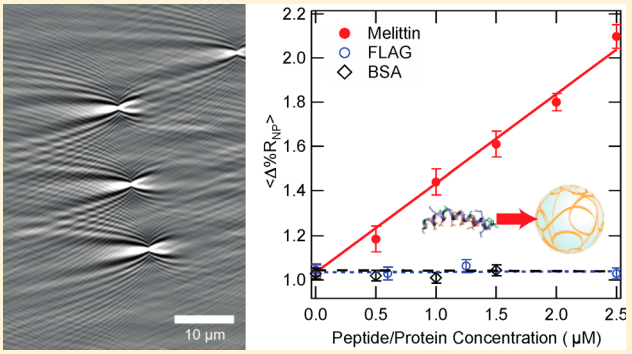

Among the numerous nanoscale drug delivery systems that are currently being developed, hydrogel nanoparticles (HNPs) have become an increasingly popular vehicle for the controlled uptake, localization, and release of bioactive compounds.[1−6] These polymeric nanoparticles can be engineered to respond to external stimuli by switching their physical properties, making them ideal candidates for the targeted delivery of therapeutics. For example, small changes in solvent pH, ionic strength, temperature, or light can drastically change an HNP's physical or chemical properties, and these changes can be used for the uptake and release of drugs, genes, peptides, or proteins.[7−11]

In addition to engineering HNPs to be sensitive to environmental changes, the polymer makeup of the nanoparticles can be tailored to uptake specific target compounds. Previously, temperature responsive HNPs were shown to reversibly switch affinity to a host of target compounds including short peptides, proteins, and drug molecules such as doxorubicin.[12−16] The affinity of HNPs to specific compounds can be controlled by reacting *N*-isopropylacrylamide (NIPAm) with polymers containing complimentary functional groups. Figure 1a depicts NIPAm-based HNPs that incorporate hydrophobic groups (*N*-*tert*-butylacrylamide, TBAm), negatively charged groups (acrylic acid, AAc), and cross-linkers (*N*,*N*′-methylenebisacrylamide, BIS). These HNPs were designed to have a high uptake affinity for melittin, the principal component of bee venom and a molecule that has shown promise in the treatment of HIV infections and epilepsy.[17,18] Melittin is a short peptide composed of 26 amino acids (GIGAVLKVLT-TGLPALISWIKRKRQQ) with mostly nonpolar or positively charged residues (illustrated in Figure 2b) and, thus, is expected to specifically absorb into the HNPs via hydrophobic and electrostatic interactions.

The characterization of HNPs can be challenging given their pliable and solvent swollen internal structure. Cryo-transmission electron microscopy (cryo-TEM) can be used to examine hydrogel size and morphology,[19,20] but the in situ measurement of the uptake of small organic molecules or peptides into individual nanoparticles poses greater challenges. Dynamic light scattering (DLS) can be used to determine mean hydrodynamic diameters of HNPs,[21] but the effect of the uptake of molecules into nanoparticles on the DLS is difficult to quantify. Multiangle light scattering (MALS) measurements have been used to estimate molecular weight changes upon protein loading by hydrogels,[22] but both DLS and MALS provide only average results for any change upon HNP loading. In addition, HNP affinity to proteins have been estimated by

Received: February 26, 2015
Accepted: April 6, 2015
Published: April 6, 2015

ACS Publications © 2015 American Chemical Society

DOI: 10.1021/acs.analchem.5b00776
Anal. Chem. 2015, 87, 4973−4979

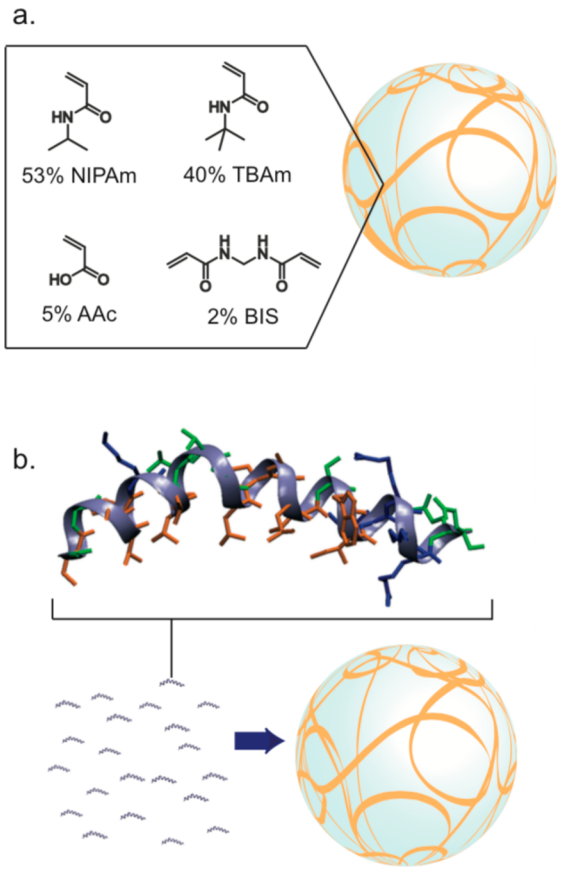

Figure 1. (a) Hydrogel nanoparticles (HNPs) were composed of *N*-isopropylacrylamide (NIPAm), *N*-*tert*-butylacrylamide (TBAm), acrylic acid (AAc), and *N*,*N*′-methylenebisacrylamide (BIS) in a molar ratio of NIPAm/TBAm/AAc/BIS: 53:40:5:2. (b) Illustration of melittin with nonpolar side chains in orange, polar side chains in green, and positively charged side chains in blue. Melittin is bound by HNPs via hydrophobic and electrostatic interactions (melittin structure obtained from the Research Collaboratory for Structural Bioinformatics).

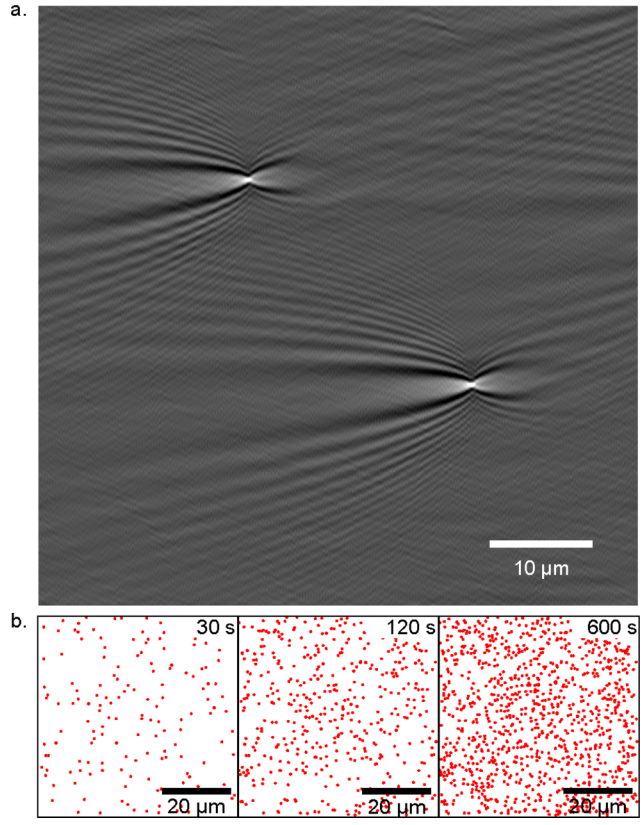

Figure 2. (a) A 58.5 μm × 58.5 μm Fourier filtered SPRM three second differential reflectivity image showing the adsorption of two individual 220 nm diameter HNPs onto a C11-functionalized gold thin film from a 30 pM HNP PBS solution. (b) Three 2-D cumulative adsorption maps tracking the locations of adsorbed HNPs after 30, 120, and 600 s in the same imaging area. Each red point corresponds to the adsorption of a single HNP. The total cumulative number of adsorbed HNPs after 30, 120, and 600 s is 152, 448, and 1051 nanoparticles, respectively.

size exclusion chromatography,[23] but the interpretation of elution data is nontrivial.

Single nanoparticle surface plasmon resonance microscopy (SPRM) is a relatively new technique that uses surface plasmon polariton (SPP) point diffraction patterns to monitor in real-time the adsorption of single nanoparticles onto a gold surface.[24−26] In addition to single nanoparticles, SPRM has been employed to study a variety of nanostructures, membrane proteins, intracellular processes, cell−substrate interactions, and viruses.[27−34] In a recent paper, we showed that near-infrared (NIR, 814 nm) SPRM is highly sensitive and can be used to track the adsorption of individual gold and polystyrene nanoparticles onto chemically modified gold thin film surfaces in real time.[35] Upon adsorption of a nanoparticle, a large SPP point diffraction pattern on the order of 10^2 μm^2 is generated; the magnitude of the response depends on the size and composition of the nanoparticle and has been observed for both gold nanoparticles as small as 20 nm and polystyrene nanoparticles as small as 85 nm.

In this paper, the uptake of the bioactive peptide melittin into NIPAm-based HNPs is directly measured with NIR SPRM. As noted above, the NIPAm-based HNPs contain a mixture of hydrophobic and negatively charged side chains that provide a specific affinity for the peptide melittin. The adsorption of single 220 nm HNPs from picomolar nanoparticle solutions onto a hydrophobic alkanethiol-modified gold surface is detected in real-time from the appearance of point diffraction patterns in sequential SPR differential reflectivity images; these point diffraction patterns are counted to create a digital adsorption binding curve. The intensities of the point diffraction patterns observed in the sequential SPR differential reflectivity images used to create this digital adsorption binding curve are quantitated, and the average of these intensity values, denoted as $\langle \Delta\%R_{NP} \rangle$, is obtained. When melittin is mixed at micromolar concentrations with the HNPs, the value of $\langle \Delta\% R_{NP} \rangle$ is found to increase linearly with melittin concentration. This increase is attributed to an increase in the refractive index of the HNPs due to the incorporation of melittin into the hydrogel nanoparticle. DLS measurements confirm that no change in mean HNP hydrodynamic diameter is observed in the presence of melittin over this entire concentration range, indicating that the increase of the SPRM response is not from a volume increase. The specific uptake affinity of melittin for these HNPs is confirmed as no increase in $\langle \Delta\%R_{NP} \rangle$ is observed in the presence of micromolar solutions of either FLAG octapeptide or bovine serum albumin (BSA). Additional bulk fluorescence measurements that measure the loss of melittin in solution when mixed with HNPs are used to

DOI: 10.1021/acs.analchem.5b00776
Anal. Chem. 2015, 87, 4973−4979

estimate that a 1% increase in $\langle \Delta\%R_{NP} \rangle$ corresponds to the uptake of approximately 65000 molecules into the 220 nm HNP, corresponding to roughly 4% of its volume.

EXPERIMENTAL CONSIDERATIONS

Hydrogel Nanoparticle Materials. All chemicals were obtained from commercial sources: *N*-isopropylacrylamide (NIPAm) and ammonium persulfate (APS) were from Sigma-Aldrich, Inc. (St. Louis, MO); acrylic acid (AAc) and sodium dodecyl sulfate (SDS) were from Aldrich Chemical Co.; *N*,*N*′-methylenebisacrylamide (BIS) was from Fluka; *N*-*tert*-butylacrylamide (TBAm) was from Acros Organics (Geel, Belgium).

Hydrogel Nanoparticle Synthesis. The procedure reported by Debord and Lyon was adapted to synthesize HNPs.[36] AAc (5 mol %), TBAm (40 mol %), NIPAm (53 mol %), BIS (2 mol %), and SDS (2.5 mg) were dissolved in water (50 mL) and the resulting solutions were filtered through a No. 2 Whatman filter paper. TBAm was dissolved in ethanol (1 mL) before addition to the monomer solution. The total monomer concentration was 65 mM. Nitrogen gas was bubbled through the reaction mixtures for 30 min. Following the addition of 500 μL of aqueous solution containing 30 mg of APS, the prepolymerization mixture was sealed under nitrogen gas. Polymerization was carried out by inserting the round bottle flask containing prepolymerization mixture in an oil bath preset to 60 °C for 3 h. The polymerized solutions were purified by dialysis using a 12−14 kDa molecular weight cut off (MWCO) membrane against an excess amount of pure water (changed more than twice a day) for 4 days. The yield and concentration of HNPs were determined by gravimetric analysis of lyophilized polymers.

Dynamic Light Scattering Measurements. The hydrodynamic diameter of HNPs was determined in aqueous solutions (25 ± 0.1 °C) by a dynamic light scattering (DLS) instrument equipped with Zetasizer Software Ver. 6.12 (Zetasizer Nano ZS, Malvern Instruments Ltd., Worcestershire, U.K.). All the results of DLS data fitting met the quality criteria set by Malvern (see Supporting Information for DLS results).

d*n*/d*c* and MALS Measurements. The average molar mass of the HNPs was determined by a combination of d*n*/d*c* and multiangle light scattering (MALS) measurements using Optilab rEX (Wyatt Technology Corporation, Santa Barbara, CA) and DAWN HELEOS (Wyatt Technology Corporation), respectively (see Supporting Information for details).

Surface Plasmon Resonance Microscope Optical Setup. The SPR microscope setup was discussed in a recent publication and diagrammed in the Supporting Information.[35] Briefly, the microscope was built into the frame of an IX51 inverted microscope (Olympus, Tokyo, Japan). A 1 mW 814 nm diode laser (Melles Griot, Carlsbad, CA) was expanded and collimated using a spatial filter (Newport Corp., Newport Beach, CA). The beam was then polarized and focused with a lens (f = 200 mm) onto the back focal plane of a 100× 1.49 NA oil objective (Olympus). The focused beam was directed up to the objective using a gold-coated knife-edge mirror (Thorlabs, Newton, NJ). The reflected image was passed to an Andor Neo sCMOS (South Windsor, CT). Images were acquired by accumulating 30 11-bit exposures.

Substrate Preparation. Substrates were borosilicate No. 1.5 coverslips (Fisherbrand, Pittsburgh, PA) coated with 1 nm Cr adhesion layer and 45 nm Au by thermal evaporation. The Au surface was functionalized by undecanethiol (C11) by overnight immersion of the substrate in a 1 mM ethanolic solution of 1-undecanethiol (Sigma-Aldrich). The imaging surface was partitioned using adhesive silicone isolation wells (Electron Microscopy Sciences, Hatfield, PA).

SPRM Analysis. HNP solutions were prepared by a 50-fold dilution in 1× PBS (11.9 mM phosphates, 137 mM sodium chloride, 2.7 mM potassium chloride, pH 7.4, Fisher). For SPRM measurements, the HNPs were further diluted by 3/10 with 1× PBS and the appropriate amount of 9 μM melittin (Sigma-Aldrich), FLAG peptide (DYKDDDDK, Sigma-Aldrich), or bovine serum albumin (Sigma-Aldrich) in PBS, which yielded a solution with a final HNP concentration of 30 pM. Images were acquired after 5 min of mixing the HNP and melittin. A total of 10 μL of HNP solution was pipetted into the isolation well for imaging. In this work, the $\Delta\%R$ from the adsorption of a nanoparticle was calculated by multiplying the quotient of the difference image and raw image by 30% (the incidence angle was set to 30% reflectivity):[35]

$$\Delta\%R = \frac{p_{i+1} - p_i}{p_i} \times 30\%$$

where p_i is the pixel intensity in frame i.

Bulk Melittin Fluorescence Measurements. The intrinsic fluorescence of melittin from its sole tryptophan residue[37] was measured for bulk uptake measurements. Duplicate 5 mL samples were prepared with and without HNPs in the same concentrations as for SPRM analysis. All samples were ultracentrifuged (50000 rpm, 1 h) using a Beckman Coulter Optima LE-80K Ultracentrifuge (Beckman Coulter, Inc., Brea, CA) with a NVT90 rotor (Beckman Coulter). The supernatant was then removed for fluorescence measurements using a JASCO FP-6300 Spectrofluorometer (JASCO Analytical Instruments, Easton, MD). Fluorescence was measured for samples with and without melittin to determine a percent loss of melittin upon mixing with HNPs. For 0.5 μM melittin samples, the supernatant was removed upon ultracentrifugation and lyophilized using FreeZone 4.5 (Labconco, Kansas City, MO); these samples were then dissolved in 1/10 of the original volume to obtain 10× concentrated samples. Fluorescence measurements are detailed in the Supporting Information.

RESULTS AND DISCUSSION

A. Synthesis of 220 nm NIPAm-Based HNPs for Melittin Uptake. As depicted in Figure 1a, HNPs were synthesized by the copolymerization of four monomers: *N*-isopropylacrylamide (NIPAm), *N*-*tert*-butylacrylamide (TBAm), acrylic acid (AAc), and *N*,*N*′-methylenebisacrylamide with molar percentages of 53, 40, 5, and 2%, respectively. The mean hydrodynamic diameter of these HNPs in phosphate buffered saline (PBS) solution was determined by DLS measurements to be 220 nm. Additional d*n*/d*c* and multiangle light scattering measurements were used to obtain an estimate of (1.24 ± 0.04) × 10^9 g/mol for the average molecular weight of the HNPs (see Supporting Information for the details of these measurements). Using this average molecular weight and an approximate dry polymer density of 1.1 g/mL (which is equivalent to the density of NIPAm),[38] we estimate that the HNPs contain approximately ∼65% solvent (in this case, PBS) by volume. The high percentage TBAm incorporated into the HNPs makes them very nonpolar, and the inclusion of AAc residues gives the HNPs a net negative charge in PBS. These

DOI: 10.1021/acs.analchem.5b00776
Anal. Chem. 2015, 87, 4973−4979

HNPs are expected to have a specific uptake affinity for melittin, which has 16 nonpolar, 5 polar, and 5 charged amino acid residues with a net charge of +6 in PBS[39,40] via a combination of hydrophobic and electrostatic interactions.[12,13]

B. Irreversible Adsorption of Single 220 nm HNPs onto a Hydrophobic Surface. Because of their significant nonpolar nature, the HNPs were found to irreversibly adsorb from PBS solutions onto gold surfaces that had been previously modified with hydrophobic undecanethiol (C11) monolayers. Real-time single nanoparticle SPRM measurements were employed to monitor the adsorption of 220 nm HNPs onto C11-functionalized gold surfaces. Specifically, 10 μL of a 15, 30, or 60 pM HNP solution was pipetted onto a C11-functionalized gold thin film, and SPRM reflectivity images were recorded every three seconds for a total of 10 min. For each SPRM reflectivity image, the SPRM reflectivity image from the immediately previous time frame was subtracted in order to create a time course series of SPRM differential reflectivity images. An example of one of these SPRM differential reflectivity images for adsorption from a 30 pM HNP solution is shown in Figure 2a.

As reported previously by a number of research groups,[24−26,35] the adsorption of single metal, semiconductor, and polymer nanoparticles onto a gold thin film can appear in the SPRM differential reflectivity image as point diffraction patterns of the surface plasmon polaritons (SPPs) traveling across the surface. In Figure 2a, two point diffraction patterns are clearly visible due to the adsorption of single HNPs. These diffraction patterns are very similar to those we have seen previously with gold nanoparticles and polystyrene nanoparticles, and are due to constructive and destructive interferences created in the 814 nm traveling SPP waves by the change in local refractive index due to the adsorption of a 220 nm nanoparticle. The total size of the image in Figure 2a is 58.5 μm × 58.5 μm, and remarkably, the signal created from one low density 220 nm nanoparticle can span more than a 10 μm × 10 μm area in this image. The two distinct diffraction patterns in Figure 2a signify that two HNPs have adsorbed onto the imaging area in this three second time frame. SPRM differential reflectivity images have also been used to monitor the desorption of nanoparticles from the surface, which appear as negative images in these diffraction patterns.[35] However, no desorption events were observed in the differential reflectivity images for HNP adsorption onto C11-functionalized surfaces, indicating that the hydrophobicity of the HNPs was sufficient to irreversibly adsorb the nanoparticles over the time frame of 10 min.

The number and locations of adsorbed nanoparticles were recorded for each SPRM differential reflectivity image in the time course series. Figure 2b displays three 2-D cumulative adsorption maps that plot with red points the locations of all of the 220 nm HNPs that have been adsorbed in the imaging area from a 30 pM HNP solution after 30, 120, and 600 s. These 2-D maps show that the adsorption of the HNPs onto C11-functionalized surfaces is fairly uniform and that there is no surface aggregation of the HNPs. At the concentrations used in this work, we did not observe single nanoparticle point diffraction patterns less than ~2 μm (30 pixels) apart in any given differential reflectivity image. We also did not observe any evidence of HNP aggregation, which would lead to the appearance of significantly larger point diffraction patterns. The total cumulative number of nanoparticles adsorbed to the surface after 30, 120, and 600 s was 152, 448, and 1051 nanoparticles, respectively.

By tallying this total cumulative number of adsorbed nanoparticles on a frame-by-frame basis, we are able to create "digital adsorption curves" for the adsorption of HNPs onto C11-functionalized surfaces. Figure 3 plots the cumulative

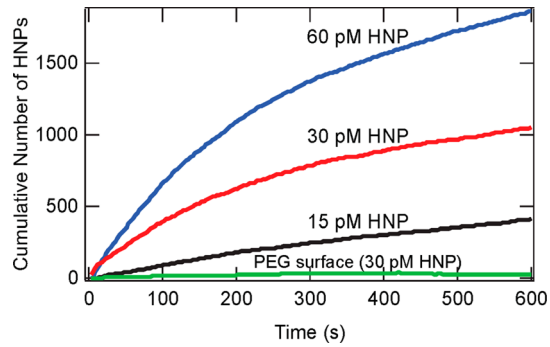

Figure 3. Real-time digital adsorption curves of the cumulative number of HNPs adsorbed onto a C11-functionalized gold surface over 10 min from 15, 30 and 60 pM HNP solutions (black, red and blue curves, respectively). The initial adsorption rates (the slopes of these curves at zero time) varied linearly with HNP concentration. Also shown in the figure is a negative control, the adsorption of HNPs from a 30 pM solution onto a PEG-functionalized gold surface (green curve) that resulted in a cumulative adsorption of less than 20 HNPs in 10 min.

number of adsorbed 220 nm HNPs of 15, 30, and 60 pM concentrations over the course of 10 min. As seen in the figure, the initial adsorption rate (the slope at zero time of the adsorption curves) roughly doubles as the solution concentration doubles, as expected.[35] Also shown in the figure is the digital adsorption curve obtained after exposure of a polyethylene glycol (PEG)-functionalized gold thin film to a 30 pM HNP solution. Almost no HNP adsorption (less than 20 HNPs in 10 min) was observed onto this surface, verifying that it is a hydrophobic interaction that drives the HNPs to the C11-functionalized surface.

C. Quantitation of the Average Single Nanoparticle SPRM Reflectivity Change ($\langle\Delta\%R_{NP}\rangle$) for HNPs. In addition to counting the number of adsorbed HNPs with our digital binding curves, we are also able to quantitate the average intensity of the point diffraction patterns in the SPRM differential reflectivity images due to the adsorption of single HNPs onto the C11-functionalized surface. A false colored enlargement of one of these point diffraction images is shown in Figure 4. The signal is composed of an SPP diffraction pattern of alternating bright and dark tails and an intense central spike in the differential reflectivity ($\Delta\%R$) at the intersection of the two white dotted lines. On the right-hand side of Figure 4 is a blow up of this feature; we define the "single nanoparticle SPRM reflectivity change" ($\Delta\%R_{NP}$) as the average of the $\Delta\%R$ values for the nine pixels (a 3 × 3 array) in the image at and around the pixel with the maximum $\Delta\%R$ intensity.

To determine the average value of $\Delta\%R_{NP}$ during an HNP adsorption experiment, which we denote as $\langle\Delta\%R_{NP}\rangle$, we measured the individual $\Delta\%R_{NP}$ values for a large number of the adsorbed HNPs observed in the time course series of SPRM three second differential reflectivity images. An example of this data for the adsorption of HNPs onto a C11-

DOI: 10.1021/acs.analchem.5b00776
Anal. Chem. 2015, 87, 4973−4979

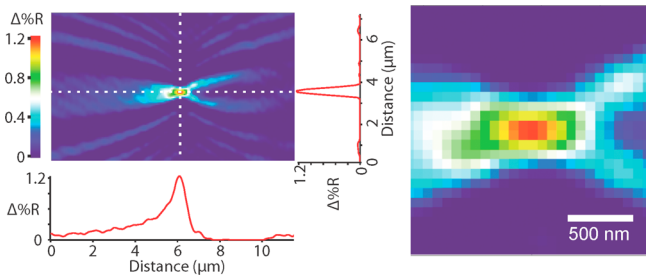

Figure 4. Determination of the single nanoparticle SPRM reflectivity change, $\Delta\%R_{NP}$, from an HNP point diffraction pattern in the SPRM three second differential reflectivity image. A sharp central feature is observed in the image at the intersection of the two white dashed lines; a blow up of that intersection is shown on the right. We define $\Delta\%R_{NP}$ as the average of the $\Delta\%R$ values for the nine pixels in the image at and around the pixel with the maximum $\Delta\%R$ intensity.

functionalized surface from a 30 pM HNP solution is plotted in Figure 5 along with the digital adsorption curve of the

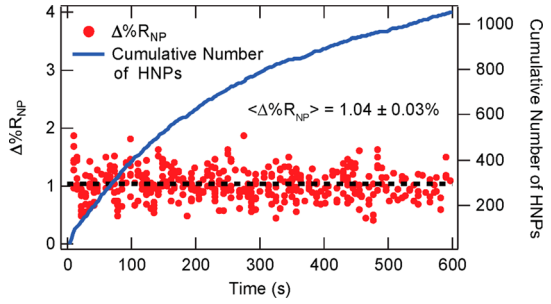

Figure 5. Determination of $\langle\Delta\%R_{NP}\rangle$ for the adsorption of 220 nm HNPs onto a C11-functionalized surface from a 30 pM HNP solution. Each red point in the plot is a $\Delta\%R_{NP}$ for a single adsorbed HNP obtained from one of the sequential SPRM differential reflectivity images. For this experiment, a total of 422 $\Delta\%R_{NP}$ values were obtained over ten minutes. The black dashed line is the value of $\langle\Delta\%R_{NP}\rangle$ obtained from this data, 1.04 ± 0.03%, where ±0.03% is the 95% confidence interval. Also plotted in the figure is the digital adsorption curve of the cumulative number of adsorbed HNPs (solid blue line).

cumulative number of adsorbed HNPs. For these experiments, we chose to work with 30 pM HNP solutions because the HNP adsorption rate at this concentration produced many images with a small number of nonoverlapping diffraction patterns. Each red dot in Figure 5 represents a $\Delta\%R_{NP}$ value obtained from a single HNP point diffraction pattern; we often obtained multiple $\Delta\%R_{NP}$ values from each differential reflectivity image. After 10 min, we measured $\Delta\%R_{NP}$ for 422 nanoparticles to obtain a $\langle\Delta\%R_{NP}\rangle$ of 1.04 ± 0.03%, where 0.03% is the value of the 95% confidence interval $(\pm 2\sigma/(422)^{1/2})$ with a standard deviation σ = 0.3%. As discussed in a previous paper,[35] the distribution in $\Delta\%R_{NP}$ values is the result of the combination of the distribution of nanoparticle sizes and any instrumental noise artifacts introduced by the SPR microscope. This measurement of $\langle\Delta\%R_{NP}\rangle$ was repeated three times, all of which yielded $\langle\Delta\%R_{NP}\rangle$ values within the confidence interval (1.04 ± 0.03%). This $\Delta\%R$ is well within the range of $\Delta\%R$ values that are regularly measured in standard SPR imaging measurements.[41−43]

D. Measurement of Melittin Uptake into HNPs via the Increase $\langle\Delta\%R_{NP}\rangle$. The NIPAm-based HNPs used in the single nanoparticle SPRM measurements have been specifically designed for the selective uptake of the bioactive 26-residue peptide melittin, and the affinity of melittin to these HNPs has been documented previously.[44] We show here that quantitative measurements of $\langle\Delta\%R_{NP}\rangle$ from single nanoparticle SPRM measurements of HNPs can be used to (i) demonstrate the specificity of melittin binding to these HNPs and (ii) quantify the amount of peptide uptake into HNPs.

The lower panel of Figure 6 plots the values of $\langle\Delta\%R_{NP}\rangle$ obtained from single nanoparticle SPRM measurements of the

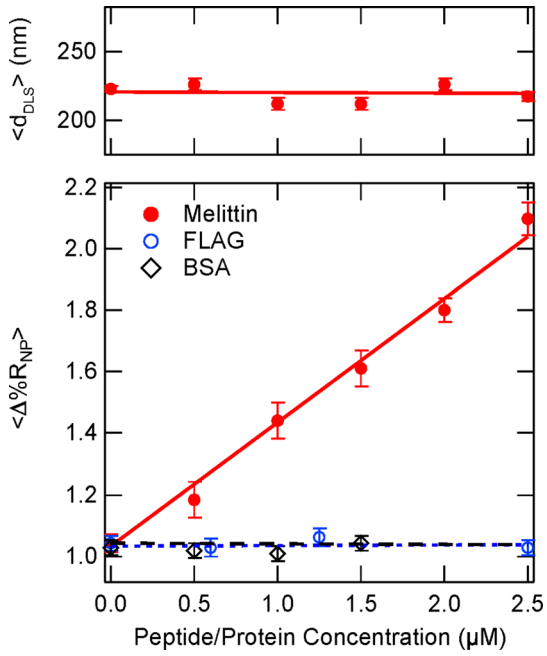

Figure 6. Lower Panel: Average single nanoparticle SPRM reflectivity values, $\langle\Delta\%R_{NP}\rangle$, obtained from single nanoparticle SPRM measurements of the adsorption of 220 nm HNPs onto C11-functionalized gold surfaces in the presence of melittin (red solid circles), FLAG peptide (blue open circles), and BSA (black open diamonds). For all measurements, the HNP concentration was fixed at 30 pM. Error bars are the 95% confidence intervals for the $\langle\Delta\%R_{NP}\rangle$ values. Upper Panel: Mean hydrodynamic diameter ($\langle d_{DLS}\rangle$) obtained from DLS measurements in the presence of melittin. The observation of no change in $\langle d_{DLS}\rangle$ in the presence of melittin confirms that the increase in $\langle\Delta\%R_{NP}\rangle$ in the presence of melittin is the result of an increase in the refractive index of the NIPAm-based HNPs due to the specific uptake of peptide molecules.

adsorption of 220 nm HNPs onto C11-functionalized gold surfaces in the presence of melittin in solution (red solid circles). At least 300 $\Delta\%R_{NP}$ values were averaged for each point in the figure. The solution concentration of the HNPs was fixed at 30 pM for all of these measurements, and the melittin concentration was varied from zero to 2.5 μM. Above 3 μM, the NIPAm-based HNPs begin to form aggregates, which have much larger SPRM responses ($\Delta\%R_{NP}$ > 4%). This aggregation is evident in DLS measurements[45] and also leads to large standard deviations in the single nanoparticle $\Delta\%R_{NP}$ values (please see the Supporting Information for more details). As seen in the figure, below 3 μM, the $\langle\Delta\%R_{NP}\rangle$ values increase linearly with the concentration of melittin. The error bars on the $\langle\Delta\%R_{NP}\rangle$ values in Figure 6 are the 95% confidence intervals; all of these $\langle\Delta\%R_{NP}\rangle$ values, standard deviations, and confidence levels are listed in Table S-1 in the Supporting Information.

DOI: 10.1021/acs.analchem.5b00776
Anal. Chem. 2015, 87, 4973−4979

Also plotted in the lower panel of Figure 6 are the values of $\langle \Delta\%R_{NP} \rangle$ obtained from single nanoparticle SPRM measurements in the presence of micromolar concentrations of FLAG octapeptide (blue open circles) and BSA (black open diamonds). No change is observed in $\langle \Delta\%R_{NP} \rangle$ in the presence of either of these molecules. The lack of interaction of the NIPAm-based HNPs with BSA has been shown previously HNPs.[44] These two additional measurements demonstrate the specificity of the melittin uptake into these HNPs.

The upper panel in Figure 6 plots the mean hydrodynamic diameters ($\langle d_{DLS} \rangle$) obtained from separate DLS measurements of the HNPs in micromolar melittin solutions (same concentrations as those used in SPRM measurements). It is clear from the figure that $\langle d_{DLS} \rangle$ does not change in the presence of melittin. Using these results, we conclude that the linear increase of $\langle \Delta\%R_{NP} \rangle$ with melittin concentration observed for the HNPs in the single nanoparticle SPRM measurements is due to an increase in the refractive index of NIPAm-based HNPs created by the uptake of melittin peptides which replace the lower refractive index PBS.

E. Quantitation of the Single Nanoparticle SPRM Response with Bulk Solution Loss Fluorescence Measurements. In order to estimate the sensitivity of the single nanoparticle SPRM measurements toward melittin uptake into HNPs, we also performed a set of "solution loss" measurements to roughly measure the average number of melittin molecules absorbed per nanoparticle. In these experiments, the total amount of melittin removed from solution after mixing with HNPs is measured by the decrease in the intrinsic fluorescence of the melittin in solution.[37] The same concentrations of HNPs and melittin that were used in SPRM experiments were also used for these fluorescence experiments, but in a greater total solution volume of 5.0 mL. These measurements require ultracentrifugation to separate the HNPs from the supernatant; in addition, lower concentrations of melittin required a lyophilization and concentration step to detect a quantifiable fluorescence signal. Nevertheless, in these solution loss experiments, a measureable decrease in fluorescence signal was observed, and, from the calculated concentration changes and the total solution volume, the number of moles of melittin removed from the solution by absorption into the HNPs in the bulk measurements could be estimated (please see Supporting Information). Dividing this number by the number of moles of HNPs in these solutions (30 pM × 5.0 mL = 150 fmol) yields an approximate value for the average number of melittin molecules absorbed per HNP. These values are plotted in Figure 7 (open blue circles) as a function of melittin concentration along with the $\langle \Delta\%R_{NP} \rangle$ values from the single nanoparticle SPRM measurements from Figure 6 (filled red circles). Both plots are linear with melittin concentration from zero to 2.5 μM.

Using the two sets of measurements plotted in Figure 7, the sensitivity of the single nanoparticle SPRM response can be quantitated. A 1% increase in $\langle \Delta\%R_{NP} \rangle$ roughly corresponds to the maximum loading of 65000 melittin molecules into each 220 nm HNP. If we estimate the volume occupied by a melittin molecule to be 3.445 nm^3,[46] then 65000 molecules is approximately 4% of the total volume of the 220 nm diameter HNP. Using the molecular weight of melittin (2846.5 g/mol) and the molecular weight of the HNPs estimated from dn/dc and MALS measurements (1.24 × 10^9 g/mol), the maximum mass ratio of melittin to polymer observed in these 220 nm HNPs is 15%.

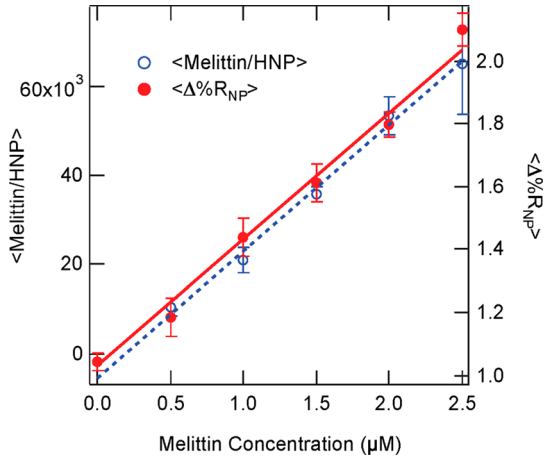

Figure 7. Average number of melittin molecules absorbed per HNP, as determined from solution loss fluorescence measurements (open blue circles) and $\langle \Delta\%R_{NP} \rangle$ values from single nanoparticle SPRM measurements (solid red circles) as a function of melittin concentration in solution. The HNP concentration in these measurements was fixed at 30 pM. Using these measurements, a 1% increase in $\langle \Delta\%R_{NP} \rangle$ corresponds to the loading of 65000 melittin molecules into each HNP. The lowest detected amount of melittin loading with single nanoparticle SPRM measurements was an increase in $\langle \Delta\%R_{NP} \rangle$ of 0.15% or approximately 10000 melittin molecules.

The lowest detected amount of melittin loading observed in the single nanoparticle SPRM measurements is an increase in $\langle \Delta\%R_{NP} \rangle$ of 0.15% or approximately 10000 melittin molecules per HNP. This corresponds to 0.6% of the volume of the 220 nm HNP and a melittin/polymer mass ratio of 2.0%. As mentioned above, these bulk solution estimates assume that no melittin is lost to cell walls during ultracentrifugation and lyophilization and that the ultracentrifugation process does not alter the melittin uptake equilibrium. Despite these caveats, the ability to detect the incorporation of 10000 melittin molecules into a single 220 nm nanoparticle attests to the high sensitivity of these unique SPRM measurements that only rely on the refractive index of the analyte.

CONCLUSIONS AND FUTURE DIRECTIONS

In this paper we have demonstrated that quantitative single nanoparticle SPRM measurements can be used to measure in situ the uptake of the bioactive peptide melittin into single HNPs. The average single nanoparticle SPRM reflectivity change $\langle \Delta\%R_{NP} \rangle$ is measured during the adsorption of 220 nm NIPAm-based HNPs onto C11-functionalized gold surfaces from the quantitative analysis of hundreds of single nanoparticle point diffraction patterns in sequential SPRM differential reflectivity images that are collected in real-time during the adsorption process. The value of $\langle \Delta\%R_{NP} \rangle$ increases linearly with melittin concentrations up to 2.5 μM due to the uptake of peptide molecules into the HNPs that results in an increased nanoparticle refractive index. The SPRM response can be roughly calibrated using bulk fluorescence solution loss measurements; the maximum loading into the 220 nm HNPs that we observe with the single nanoparticle SPRM measurements corresponds to the uptake of approximately 65000 melittin molecules or 4% of the nanoparticle volume. The minimum change in $\langle \Delta\%R_{NP} \rangle$ that we detect corresponds to approximately 10000 melittin molecules or 0.6% of the nanoparticle volume.

DOI: 10.1021/acs.analchem.5b00776
Anal. Chem. 2015, 87, 4973−4979

In the future, in addition to quantitating the specific uptake of melittin into the HNPs, these digital SPRM measurements can also be used to study the real-time adsorption of HNPs to bioactive surfaces, and also potentially to monitor melittin release from adsorbed monolayers of HNPs. As our SPRM measurements of single nanoparticle point diffraction patterns improve, we will also begin to examine the single $\Delta\%R_{NP}$ values in order to obtain additional information about the distribution characteristics of single HNPs. These single nanoparticle SPRM measurements are a direct measure of peptide uptake into the soft hydrogel nanoparticle via the refractive index of the molecule and potentially can be applied to the uptake of other peptides, proteins, and drug molecules into various porous nanoparticles and mesoparticles, such as dendrimers, porous silica nanoparticles, and liposomes.

■ ASSOCIATED CONTENT

Supporting Information

Diagram of optical setup of the SPR microscope, HNP synthesis and characterization information, and other experimental details. This material is available free of charge via the Internet at http://pubs.acs.org.

■ AUTHOR INFORMATION

Corresponding Author

*E-mail: rcorn@uci.edu.

Notes

The authors declare no competing financial interest.

■ ACKNOWLEDGMENTS

This work was supported by the National Institutes of Health through Grant GM059622 (R.M.C.) and the National Science Foundation through Grant DMR-1308363 (K.J.S.). The authors thank Dr. Aaron Halpern for guidance and helpful discussions on the use of SPRM and Dr. Kotaro Azuma, Dr. Takashige Kawakami, and the Blumberg group at UC Irvine for the use of their ultracentrifuge.

■ REFERENCES

(1) Agarwal, R.; Singh, V.; Jurney, P.; Shi, L.; Sreenivasan, S. V.; Roy, K. *ACS Nano* **2012**, *6*, 2524−2531.

(2) Hamidi, M.; Azadi, A.; Rafiei, P. *Adv. Drug Delivery Rev.* **2008**, *60*, 1638−1649.

(3) Soppimath, K. S.; Aminabhavi, T. M.; Kulkarni, A. R.; Rudzinski, W. E. *J. Controlled Release* **2001**, *70*, 1−20.

(4) Peppas, N. A.; Hilt, J. Z.; Khademhosseini, A.; Langer, R. *Adv. Mater.* **2006**, *18*, 1345−1360.

(5) Kabanov, A. V.; Vinogradov, S. V. *Angew. Chem., Int. Ed.* **2009**, *48*, 5418−5429.

(6) Vermonden, T.; Censi, R.; Hennink, W. E. *Chem. Rev.* **2012**, *112*, 2853−2888.

(7) Seliktar, D. *Science* **2012**, *336*, 1124−1128.

(8) Kang, H.; Liu, H.; Zhang, X.; Yan, J.; Zhu, Z.; Peng, L.; Yang, H.; Kim, Y.; Tan, W. *Langmuir* **2011**, *27*, 399−408.

(9) Raemdonck, K.; Demeester, J.; De Smedt, S. *Soft Matter* **2009**, *5*, 707−715.

(10) Smith, M. H.; Lyon, L. A. *Acc. Chem. Res.* **2012**, *45*, 985−993.

(11) Nayak, S.; Lyon, L. A. *Angew. Chem., Int. Ed.* **2005**, *44*, 7686−7708.

(12) Hoshino, Y.; Koide, H.; Urakami, T.; Kanazawa, H.; Kodama, T.; Oku, N.; Shea, K. J. *J. Am. Chem. Soc.* **2010**, *132*, 6644−6645.

(13) Hoshino, Y; Urakami, T; Kodama, T; et al. *Small* **2009**, *13*, 1562−1568.

(14) Lee, S. -H; Hoshino, Y.; Randall, A.; Zeng, Z.; Baldi, P.; Doong, R.; Shea, K. J. *J. Am. Chem. Soc.* **2012**, *134*, 15765−15772.

(15) Missirlis, D.; Kawamura, R.; Tirelli, N.; Hubbell, J. A. *Eur. J. Pharm. Sci.* **2006**, *29*, 120−129.

(16) Yoshimatsu, K.; Lesel, B. K.; Yonamine, Y.; Beierle, J. M.; Hoshino, Y.; Shea, K. J. *Angew. Chem., Int. Ed.* **2012**, *51*, 2405−2408.

(17) Soman, N. R.; Lanza, G. M.; Heuser, J. M.; Schlesinger, P. H.; Wickline, S. A. *Nano Lett.* **2008**, *8*, 1131−1136.

(18) Hood, J. L.; Jallouk, A. P.; Campbell, N.; Ratner, L.; Wickline, S. A. *Antiviral Ther.* **2013**, *18*, 95−103.

(19) Ballauff, M.; Lu, Y. *Polymer* **2007**, *48*, 1815−1823.

(20) Karg, M.; Hellweg, T. *Curr. Opin. Colloid Interface Sci.* **2009**, *14*, 438−450.

(21) Griset, A. P.; Walpole, J.; Liu, R.; Gaffey, A.; Colson, Y. L.; Grinstaff, M. W. *J. Am. Chem. Soc.* **2009**, *131*, 2469−2471.

(22) Smith, M. H.; Lyon, L. A. *Macromolecules* **2011**, *44*, 8154−8160.

(23) Cedervall, T.; Lynch, I.; Lindman, S.; Berggard, T.; Thulin, E.; Nilsson, H.; Dawson, K. A.; Linse, S. *Proc. Natl. Acad. Sci. U.S.A.* **2007**, *104*, 2050−2055.

(24) Zybin, A.; Kuritsyn, Y. A.; Gurevich, E. L.; Temchura, V. V.; Uberla, K.; Niemax, K. *Plasmonics* **2010**, *5*, 31−35.

(25) Weichert, F.; Gaspar, M.; Timm, C.; Zybin, A.; Gurevich, E. L.; Engel, M.; Muller, H.; Marwedel, P. *Sens. Actuators, B* **2010**, *151*, 281−290.

(26) Wang, S.; Shan, X.; Patel, U.; Huang, X.; Lu, J.; Li, J.; Tao, N. *Proc. Natl. Acad. Sci. U.S.A.* **2010**, *107*, 16028−16032.

(27) Rothenhausler, B.; Knoll, W. *Nature* **1988**, *332*, 615−617.

(28) Jamil, M. M.; Youseffi, M.; Twigg, P. C.; Britland, S. T.; Liu, S.; See, C. W.; Zhang, J.; Somekh, M. G.; Denyer, M. C. *Sens. Actuators, B* **2008**, *129*, 566−574.

(29) Wang, W.; Foley, K.; Shan, X.; Wang, S.; Eaton, S.; Nagaraj, V. J.; Wiktor, P.; Patel, U.; Tao, N. *Nat. Chem.* **2011**, *3*, 249−255.

(30) Wang, W.; Wang, S.; Liu, Q.; Wu, J.; Tao, N. *Langmuir* **2012**, *28*, 13373−13379.

(31) Giebel, K. -F.; Bechinger, C.; Herminghaus, S.; Riedel, M.; Leiderer, P.; Weiland, U.; Bastmeyer, M. *Biophys. J.* **1999**, *76*, 509−516.

(32) Wang, W.; Tao, N. *Anal. Chem.* **2014**, *86*, 2−14.

(33) Yu, H.; Shan, X.; Wang, S.; Chen, H.; Tao, N. *ACS Nano* **2014**, *8*, 3427−3433.

(34) Shan, X.; Díez-Pérez, I.; Wang, L.; Wiktor, P.; Gu, Y.; Zhang, L.; Wang, W.; Lu, J.; Wang, S.; Gong, Q.; Li, J.; Tao, N. *Nat. Nanotechnol.* **2012**, *7*, 668−672.

(35) Halpern, A. R.; Wood, J. B.; Wang, Y.; Corn, R. M. *ACS Nano* **2014**, *8*, 1022−1030.

(36) Debord, J. D.; Lyon, L. A. *Langmuir* **2003**, *19*, 7662−7664.

(37) Raghuraman, H.; Chattopadhyay, A. *Biophys. J.* **2004**, *87*, 2419−2432.

(38) Bae, Y. H.; Okano, T.; Kim, S. W. *J. Polym. Sci., Part B: Polym. Phys.* **1990**, *28*, 923−936.

(39) Matsuzaki, K.; Yoneyama, S.; Miyajima, K. *Biophys. J.* **1997**, *73*, 831−838.

(40) Glättli, A.; Chandrasekhar, I.; Gunsteren, W. F. *Eur. Biophys. J.* **2006**, *35*, 255−267.

(41) Chen, Y.; Nguyen, A.; Niu, L.; Corn, R. M. *Langmuir* **2009**, *25*, 5054−5060.

(42) Nelson, B. P.; Grimsrud, T. E.; Liles, M. R.; Goodman, R. M.; Corn, R. M. *Anal. Chem.* **2001**, *73*, 1−7.

(43) Guedon, P.; Livache, T.; Martin, F.; Lesbre, F.; Roget, A.; Bidan, G.; Levy, Y. *Anal. Chem.* **2000**, *72*, 6003−6009.

(44) Hoshino, Y.; Koide, H.; Furuya, K.; Haberaecker, W. W.; Lee, S. -H.; Kodama, T.; Kanazawa, H.; Oku, N.; Shea, K. J. *Proc. Natl. Acad. Sci. U.S.A.* **2012**, *109*, 33−38.

(45) Driskell, J. D.; Jones, C. A.; Tompkins, S. M.; Tripp, R. A. *Analyst* **2011**, *136*, 3083−3090.

(46) Center for Biotechnology, Northwestern University. Peptide Properties Calculator; http://www.basic.northwestern.edu/biotools/proteincalc.html (accessed Feb. 20, 2015).

DOI: 10.1021/acs.analchem.5b00776
Anal. Chem. 2015, 87, 4973−4979